Title

Orientation transitions during the growth of imine covalent organic framework thin films

Journal

Journal of Materials Chemistry C, 5(21)

ISSN

2050-7526

Authors

Wang, H

He, B

Liu, F

et al.

Publication Date

2017

DOI

10.1039/c7tc01324h

Peer reviewed

Journal of
Materials Chemistry C

PAPER

View Article Online
View Journal | View Issue

Cite this: J. Mater. Chem. C, 2017, 5, 5090

Orientation transitions during the growth of imine covalent organic framework thin films†

H. Wang,‡[abc] B. He,‡[bd] F. Liu,[d] C. Stevens,[bf] M. A. Brady,[be] S. Cai,[g] C. Wang,[e] T. P. Russell,[cdhi] T.-W. Tan*[a] and Y. Liu*[bd]

Received 28th March 2017,
Accepted 25th April 2017

DOI: 10.1039/c7tc01324h

rsc.li/materials-c

Oriented growth of thin films of covalent organic frameworks (COFs) has attracted significant interest as the anisotropically aligned channels provide ideal nanoscopic domains that can facilitate mass transport or charge percolation. Despite some experimental progress in achieving oriented COF thin films, little is known about the kinetics and thermodynamics associated with the orientation or control over the solution-based growth process. We performed a systematic study of the thin film growth of an imine-based COF as a function of concentration and growth time. Grazing incidence wide-angle X-ray scattering (GIWAXS) was used to reveal the orientation and evolution of crystallization within the thin films at sequential growth stages. An unusual re-entrant transition from an oriented to disoriented to reoriented state was discovered, which correlates with the kinetics associated with independent surface- and solution-based nucleation and growth processes, as well as reorganization of disoriented COF crystallites.

Covalent organic frameworks (COFs)[1] are a class of microcrystalline materials that have attracted great interest for their appealing structural features, such as light weight, high porosity and surface area and diverse chemical compositions.[2] Taking advantage of the periodicity endowed by the framework structure, incorporation of functional units into two-dimensional (2D) COFs can create well-defined interfaces between interpenetrating units, while maintaining high anisotropy, rendering 2D COFs a desirable architecture for infiltration of guest molecules,[3] and for charge separation and transport[4] when electroactive building blocks are used. Despite the fact that great strides have been made in the synthesis of powdery crystalline COFs, simple methods that enable the fabrication of COFs into oriented thin film forms are much needed, which are of technological relevance to leverage their properties for applications, including photovoltaics, sensors, and sorption membranes. Successes have been demonstrated in obtaining exfoliated films from COF crystallites, yet the domain size, thickness and surface coverage of the layers are less than optimal.[5] Attempts to deposit COF thin films using vapor-phase reactants have also shown limited success, resulting in films with poor coverage and large domain boundaries.[6] While a solution-based process is more desirable, solution-casting techniques typically used for linear polymers are not useful, since the COF layers are not soluble after crosslinking. As crystalline COF formation relies on thermodynamically controlled chemical reactions, usually requiring the participation of solvents, and is sometimes surface-dependent,[7] solution processes based on surface growth mechanisms are ideal where COFs are formed and deposited onto substrates from the solution of reaction precursors. Achieving control over the orientation, though, has been a long-standing challenge.[8] Dichtel and coworkers pioneered the oriented growth of boronate COF thin films on substrate-supported single layer graphene[9] in which favorable π–π stacking interactions between single-layered graphene and the COF layer were used to template the face-on growth of COFs. Bein and coworkers reported the facile formation of oriented thin films of large-pore boronate COFs on different substrates, and showed rapid formation upon

[a] Beijing Key Lab of Bioprocess, College of Life Science and Technology, Beijing University of Chemical Technology, Beijing 100029, China. E-mail: twtan@mail.buct.edu.cn
[b] The Molecular Foundry, Lawrence Berkeley National Laboratory, Berkeley, California 94720, USA. E-mail: yliu@lbl.gov
[c] Beijing Advanced Innovation Center for Soft Matter Science and Engineering, Beijing University of Chemical Technology, Beijing 100029, China
[d] Materials Sciences Division, Lawrence Berkeley National Laboratory, Berkeley, California 94720, USA
[e] Advanced Light Source, Lawrence Berkeley National Laboratory, Berkeley, California 94720, USA
[f] Department of Chemistry, University of California, Berkeley, Berkeley, California 94720, USA
[g] School of Chemistry and Environment, South China Normal University, Guangzhou 510006, P. R. China
[h] Department of Polymer Science and Engineering, University of Massachusetts, 120 Governors Drive, Amherst, MA 01003, USA
[i] WPI-Advanced Institute for Materials Research (WPI-AIMR), Tohoku University, 2-1-1 Katahira, Aoba, Sendai 980-8577, Japan

† Electronic supplementary information (ESI) available: GIWAXS patterns and SEM and TEM images of COF thin films. See DOI: 10.1039/c7tc01324h

‡ These authors contributed equally.

solvent annealing.[3,10] Recently the growth of boronate COF thin films was demonstrated under continuous flow conditions.[11] Oriented thin films of imine-based COFs could also be grown from conductive substrates where the preferred orientation led to COFs with high conductivity,[4d] improved photoresponse speed,[12] enhanced energy storage properties,[13] and high catalytic activity for aqueous electrochemical CO_2 reduction.[4f] While COF thin films have shown great promise, they are far from ideal in terms of orientation and domain size control, which calls for a systematic study to outline the key parameters governing COF thin film growth kinetics and anisotropic layering. In this article, we have investigated the growth of a pristine imine COF, COF-LZU1, that was first developed by Wang and coworkers,[14] by following the thin film crystallinity as a function of growth time, concentration, and substrate. Insights into the growth mechanism were obtained from detailed structural information using grazing incidence wide-angle X-ray scattering (GIWAXS), which uncovered a re-entrant orientation transition from the oriented to disoriented to reoriented state during the growth.

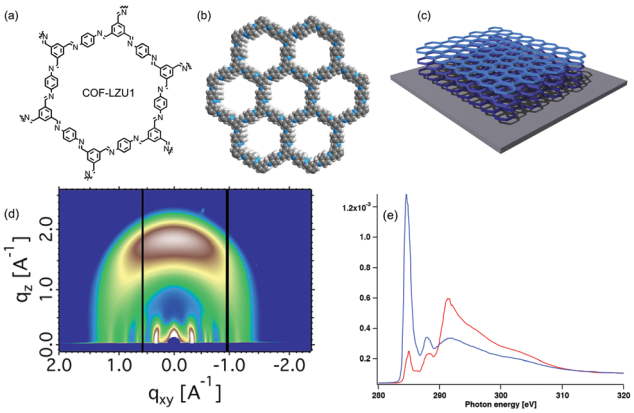

Fig. 1 (a) Molecular structure of a repeating unit of COF-LZU1. (b) In-plane hexagonal network structure of COF-LZU1. (c) Cartoon illustration of the oriented 2D COF thin films on surfaces. (d) A typical GIWAXS pattern of COF thin films grown from Si–APTES substrate. (e) NEXAFS spectra of COF thin films grown on Si–APTES at 20° incidence with *s* (red curve) and *p* (blue curve) polarization of the electric field.

Results and discussion

COF thin film growth on different surfaces

The reaction conditions for making COF-LZU1 thin films are similar to those reported for the bulk synthesis of the same COF,[14] except that substrates were introduced face down on a support rack and immersed in the reaction mixture, and the concentrations and reaction times were varied when needed (Fig. S1a in the ESI†). In a typical reaction setup, pretreated substrates (up to four) are placed in a reaction vessel that contains a degassed mixture of 1,4-diaminobenzene (DAB, 32 mg) and 1,3,5-triformylbenzene (TFB, 32 mg) (molar ratio 3 : 2) in dioxane/aqueous acetic acid (3 M) (v/v 5 : 1). A customized Teflon rack with four parallel slots is used to support up to four substrates at each time for one reaction (Fig. S1b, ESI†). The sealed reaction vessel was then placed in an oven and kept at 120 °C. The substrates retrieved from the reaction mixtures were rinsed thoroughly with acetone, DMF, and THF, and were dried at 120 °C under vacuum overnight. The above concentration was arbitrarily defined as 1-fold. Other concentrations at 0.5-, 1.5-, 2-, 2.5-, 3- and 5-fold were also employed. Glass and silicon substrates were cleaned by successive sonication in the baths of detergent solution, DI water, isopropanol, toluene and acetone. After drying under a N_2 stream, the substrates were further treated with UV–ozone for 10 min and used immediately for surface modification with self-assembled monolayers (SAMs) or directly for COF thin film growth. (3-Aminopropyl)triethoxysilane (APTES) and octadecyltrichlorosilane (OTS) modified substrates were obtained after immersing the ozone-cleaned silicon substrates in respective toluene solutions overnight.[15] The Si substrates with native silicon oxide, APTES SAM, and OTS SAM are denoted as Si–SiO_2, Si–APTES, and Si–OTS, respectively (Fig. S1c, ESI†).

Continuous thin films were grown on all three differently functionalized Si substrates with good coverage after reacting the 1-fold mixture for 48 hours, as shown by SEM images (Fig. S2, ESI†).

Further information about the internal order and orientation preferences in COF thin films was obtained from 2D GIWAXS measurement. The corresponding GIWAXS patterns (Fig. 1d and Fig. S1d–f, ESI†) showed very strong, distinctive in-plane and out-of-plane reflections in all of the thin films, suggesting a high degree of orientation. The appearance of higher order in-plane diffraction peaks is strong evidence of the high degree of internal order within the 2D COF layers. The scattering intensity variation normal to the film surface along the vertical direction, indicative of an out-of-plane cofacial stacking of the framework's conjugation planes, supports the formation of oriented COF crystallites (Fig. 1c). The locations of the sharp reflections seen in the in-plane line scans agree well with the expected 2D structure from the hexagonal imine COF-LZU1 (Fig. S3, ESI†), further confirming the formation of periodic 2D COF layers on the substrate surface. Line scans in the out-of-plane direction show a reflection corresponding to a *d*-spacing of approximately 0.35 nm, arising from the interlayer π–π stacking of the COF layers normal to the film surface. The preferential stacking orientation of COFs normal to the substrate was also confirmed by near edge X-ray absorption fine spectroscopy (NEXAFS) (Fig. 1e) where the total electron yield (TEY) profiles (corresponding to the top ~10 nm of the grown film) show an intense absorption peak at 285 eV, arising from the electronic transition from the 1s shell to the π* antibonding orbital for sp^2 carbon–carbon double bonds. The peak intensity is maximum when the electric field (**E**) of the incident X-ray is nearly normal to the substrate and minimum when **E** is parallel to the substrate. Concurrently, the peak corresponding to the σ* orbital of the C–C bond shows the opposite angular-dependence. These results are consistent with the orthogonal orientation of surface π* and σ* orbitals, which are aligned normal and parallel to the substrate, respectively. Additional transmission electron microscope (TEM) studies indicated the layered stacking of the COFs, however the in-plane hexagonal structures could not be resolved, possibly due to the instability of the pore structure under electron beam irradiation (Fig. S4, ESI†).

While COF thin films can be grown effectively on all three different substrates and show similar orientations, further analysis of the GIWAXS patterns shows that their azimuthal distribution of the out-of-plane diffraction peaks is different, with those grown from the Si–APTES substrates showing the narrowest distribution and those from Si–SiO_2 showing the broadest (Fig. S1d–f, ESI†). It suggests that the amine-terminated APTES SAM is the most effective in directing the oriented growth of COF thin films, presumably due to a higher concentration of reactive surface amine groups that take part in COF formation, and is thus chosen for the subsequent studies unless otherwise noted.

Concentration- and time-dependence

Different films on Si–APTES substrates were obtained after 48 hours of reaction based on 0.5-, 1-, 1.5-, 2-, 2.5-, and 3-fold starting material concentrations. The film thickness measured by both cross-section scanning electron microscopy (SEM) (Fig. S5, ESI†) and surface profilometry revealed a monotonic increase of film thickness with respect to concentration except at a concentration below 1-fold (Fig. 2h). GIWAXS studies show that the thin film grown from 0.5-fold concentration is amorphous, as evidenced from the amorphous scattering halo at $q \sim 1.5$ A^{-1} (Fig. 2a), corresponding to a *d*-spacing of 4.2 Å. This is consistent with the deposition of amorphous aromatic oligomers on the surface. For films grown at higher concentrations, both in-plane and out-of-plane diffraction peaks are clearly visible by GIWAXS (Fig. 2b–g). Notably for these thin films grown from concentrations between 2- and 3-fold, an azimuthally independent scattering peak is seen along with a strong in-plane (100) scattering peak, indicating the coexistence of both "face-on" oriented and randomly oriented crystallites. While the appearance of disoriented crystallites seems to correlate with higher concentrations, the films grown at 5-fold concentration show only signs of "face-on" orientation, as indicated by the absence of the ring-shaped scattering peak in the GIWAXS pattern (Fig. 2g). It should also be noted that at 5-fold concentration, the deposition of amorphous contents is more pronounced compared to the lower concentration samples, as evidence by the stronger 1.5 A^{-1} amorphous scattering halo in the diffraction profile. The concentration-dependent formation of the disoriented phase raises the question as to whether it represents a kinetically transient, metastable phase.

To gain more insights into the kinetics of the thin film growth, *ex situ* time-dependent studies were performed for two concentration series at 1.5-fold and 5-fold. For each concentration series, up to 10 reaction vessels containing identical solutions of COF precursors and Si–APTES substrates were allowed to react in parallel under identical conditions. The substrates were taken out of the reaction vessels at different time intervals and characterized following usual treatment.

At both concentrations, the film thicknesses increase monotonically with time despite the notably different rates (Fig. 3 and 4). The film thickness from 5-fold reactions increases significantly faster than those from the 1.5-fold ones, with the former reaching a thickness of 423 nm within 24 hours and the latter reaching 163 nm after 84 hours. GIWAXS studies were used to investigate the evolution of crystallinity in these thin films at different stages of the film deposition process. In particular, the combined analysis of the 2D scattering patterns, peak positions and peak widths at full width half maximum (FWHM) gave comprehensive information about crystal structures, periodicity, and crystallite sizes.[16] For the 5-fold reaction mixture, the strong out-of-plane GIWAXS peak was already developed during the first hour, concurrent with relatively weak in-plane peaks, suggesting that the COF thin films are quickly formed with a preferential coplanar orientation (Fig. 3). Both out-of-plane and in-plane peaks intensify at longer reaction times. Scattering rings at the (100) peak position, in addition to the in-plane (100) rods normal to the film surface emerged in three hours (Fig. 3b), indicate the coexistence of both oriented and disoriented polycrystalline phases in the thin film. The scattering rings gradually decreased in intensity over time and completely disappeared at t = 24 hours (Fig. 3c–f), confirming

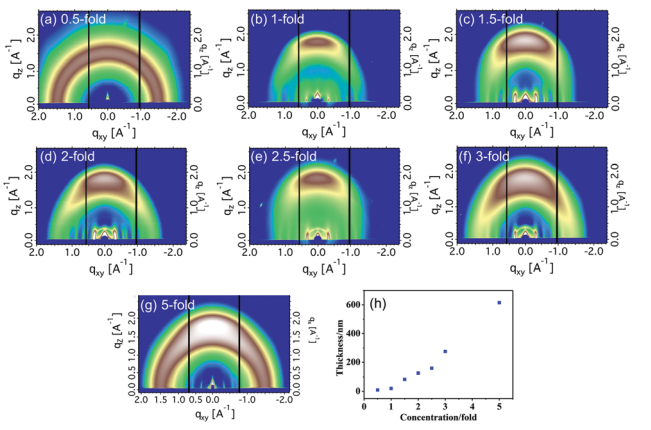

Fig. 2 GIWAXS patterns of thin films grown from different concentrations after 48 hours. (a) 0.5-fold, (b) 1-fold, (c) 1.5-fold, (d) 2-fold, (e) 2.5-fold, (f) 3-fold, (g) 5-fold. (h) Thickness of thin films plotted against different starting concentrations.

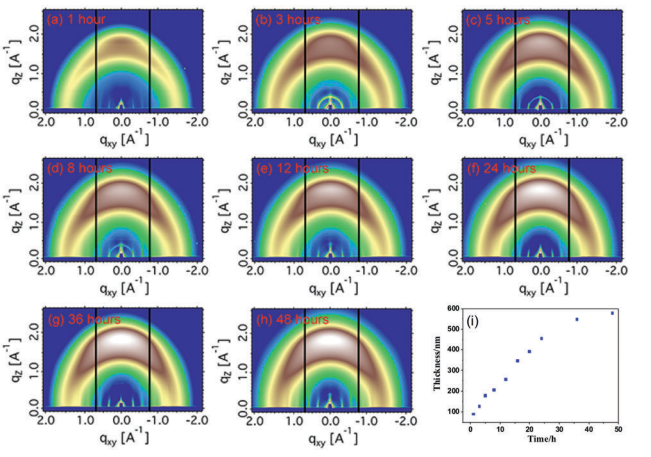

Fig. 3 GIWAXS patterns of thin films grown from 5-fold solutions at different times. (a) 1 hour, (b) 3 hours, (c) 5 hours, (d) 8 hours, (e) 12 hours, (f) 24 hours, (g) 36 hours, (h) 48 hours. (i) The plot of film thickness as a function of reaction time.

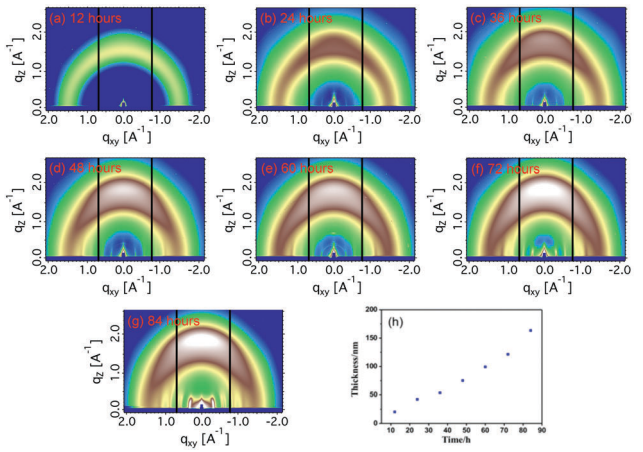

Fig. 4 GIWAXS patterns of thin films grown from 1.5-fold solutions at different times. (a) 12 hours, (b) 24 hours, (c) 36 hours, (d) 48 hours, (e) 60 hours, (f) 72 hours, (g) 84 hours. (h) The plot of film thickness as a function of reaction time.

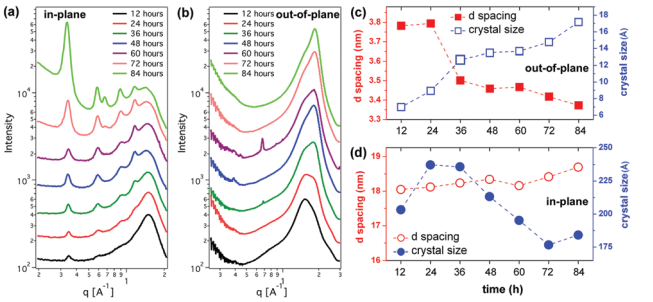

Fig. 5 Time-dependent evolution of crystalline features of COF thin films grown from 1.5-fold reactions. Stacked plots of in-plane and out-of-plane linecuts of GIWAXS profiles at different times are shown in (a) and (b), respectively. (c) Out-of-plane and (d) in-plane *d*-spacings (red spheres) and crystal sizes (blue spheres) against reaction time.

the metastability of the disoriented crystallites. This transient disoriented phase was also observed during COF thin film growth in the 1.5-fold reaction series, albeit following a much slower kinetic process. As shown in Fig. 4, the film grown after 12 hours showed evidence of a preferential vertical π–π stacking arrangement but remained largely disordered with no lateral ordering. Thin films with good in-plane ordering and orientation became more visible after 36 hours, and, after 60 hours, the disoriented intermediate phase was observed, which disappeared after 72 hours. Similar re-entrant orientation behavior transitions are observed in two separate growth series using native Si–SiO_2 substrates at 1.5-fold and 5-fold concentrations, suggesting that these are intrinsic processes during COF thin film growth and are not dependent on substrates or concentration (Fig. S6 and S7, ESI†).

The evolution of crystallinity and the metastable disoriented phase are more evident from the stacks of in-plane and out-of-plane line cuts (Fig. 5 and Fig. S8, ESI†). Taking the 1.5-fold thin film as an example, the growing intensities as a function of reaction time in both dimensions with respect to the film plane support increasing crystallinity in the thin films. A broad peak at q = 1.5 $Å^{-1}$ is observed in all of the thin films in both the in-plane and out-of-plane line cuts, which is attributed to amorphous contents co-deposited on the surface. The transient sharp peak at q = 3.3 $Å^{-1}$ originates from the (100) reflection of randomly oriented COF crystallites, a peak only observed in-plane for well oriented samples. The out-of-plane *d*-spacing from π–π stacking varies from an initial 3.8 Å formed within the first 24 hours to 3.5 Å in films developed after 36 hours (Fig. 5c), in accordance with a tighter interlayer packing in thicker films and improved ordering as the reaction proceeds. The crystal coherence length in the π–π stacking direction, calculated using the Scherrer equation,[17] showed relatively small crystallite sizes that continuously increased over time and reached 17 Å after 84 hours, which corresponds to approximately six COF layers. The in-plane *d*-spacings remain nearly constant during the thin film growth (Fig. 5d), in keeping with the stable inner layer structure. The in-plane correlation length is 200 Å ± 30 Å for the range of growth times, which is similar to the domain sizes observed by SEM studies (Fig. S9, ESI†). This agreement demonstrates that the domains observed in SEM are in fact crystalline grains of COF-LZU1.

The origin of the re-entrant transition

Ostwald's "Rule of Stages" states that crystal formation must occur through a series of intermediate crystallographic phases prior to the formation of the final thermodynamically stable structure,[18] which was previously observed in the formation of hollow COF spheres.[19] While this could explain the transition from the disoriented phase to the oriented one, the initial ordered-to-disoriented transition departs from the Ostwald step rules. Hypothesized processes for the observed transitions are shown in Fig. 6. The initially ordered phase originates with the surface-initiated film growth process that starts with the adsorption of the precursor molecules on the substrate surface. In the classical picture of nucleation, the presence of a surface results in reduced interfacial energy and lower thermodynamic barrier to nucleation, and in turn leads to kinetically faster surface nucleation than the solution-based homogeneous one (Fig. 6a).[20] The subsequent crosslinking reaction of the adsorbed precursor molecules with either the free molecules in solution or those co-adsorbed on the surface leads to the lateral growth of the initial surface layer (Fig. 6b). The appearance of amorphous films during the first 12 hours of the 1.5-fold thin film growth (Fig. 4a) indicates the formation of an initial amorphous phase, which transforms into a more crystalline phase at later reaction times (Fig. 4b–d). This is consistent with previous observations of amorphous-to-crystalline phase transformations during solution-based imine COF formation, which were attributed to the reversible nature of the dynamic imine bond by Dichtel[21] and Zhao[22] and coworkers. It should also be noted that the progressive pattern changes from Fig. 4a to d indicate the lack of any randomly oriented intermediate COF crystallites, suggesting that the amorphous phase can directly develop into oriented phases without the development of any random layer of COF crystallites, possibly through a combination

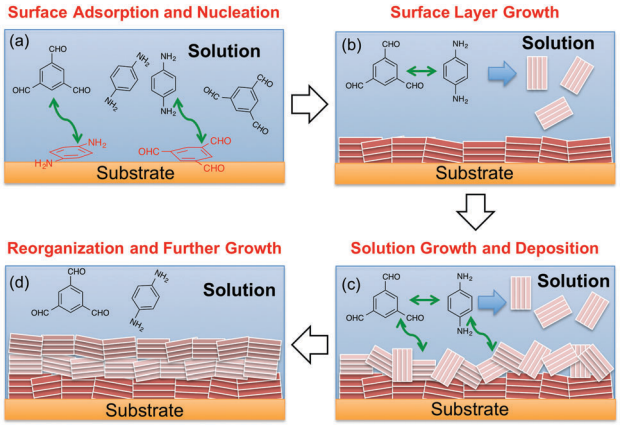

Fig. 6 Illustration of the different film growth stages. (a) Surface adsorption of precursor molecules and nucleation. (b) Surface layer growth. (c) Solution crystallite growth and deposition on top of previous surface layers. (d) Reorientation of solution deposited crystallite layers and further growth. The green double-headed arrows indicate reactions between different species.

of partial re-dissolution and templated layer growth. Accompanying the horizontal, in-plane growth of surface layers, further adsorption of aromatic precursors on the newly formed layers, presumably facilitated by favorable π–π interactions, could occur to promote out-of-plane growth of atop 2D layers in a templated fashion. A clear orientation preference of this π–π stacking in the surface normal direction is maintained in the resulting COF crystallites, while the domain size is determined by the different growth rates in the in-plane and out-of-plane directions. The stronger out-of-plane signal indicates a faster growth rate in the π-stacking direction, which negatively impacts the lateral growth to yield crystallites with limited domain sizes. This is consistent with the observations in boronate COF thin films[3] and powders grown under hydrothermal conditions.[23] The appearance of the randomly oriented COFs in the thin film strongly suggests processes other than the amorphous-to-crystalline transition within thin films, and is attributed to the deposition of solution grown crystallites, which are formed from a separate solution-based homogeneous nucleation and growth process (Fig. 6c). The decreasing lateral and increasing vertical correlation lengths of crystallites, as seen in the GIWAXS profiles in Fig. 5c and d, are also consistent with the formation of crystallites by a non-templated solution growth where vertical growth is dominant and occurs by adsorption of solution-grown crystallites onto the existing surface layers. In the film maturation stage (Fig. 6d), in addition to the formation of new top layers, rearrangement of misaligned crystallites occurs as a result of cooperative effects from (1) reversible bond breaking and formation under hydrothermal conditions and (2) the templating effect from the underlying surface layers that reinforce stacking along the surface normal. The absence of the disoriented phase in the final thin films suggests that the growth process is very adaptive and is able to reinstate a high degree of orientation after the solution deposition. To the best of our knowledge, this is the first experimental observation of a re-entrant transition in the orientation of COF thin films during the growth, which is important for the orientation of framework pores in the final thin films. Accordingly, the GIWAXS patterns shown in Fig. 2 could be well understood and represent COF thin films at four differently equilibrated stages: amorphous (0.5-fold), initially oriented (1- and 1.5-fold), intermediately disoriented (2–3-fold), and equilibrated and oriented (5-fold).

Conclusions

We have conducted a systematic study on the mechanism of thin film growth of a prototypical imine COF on modified silicon substrates. 2D GIWAXS studies provide strong evidence for the two-dimensionally oriented growth of 2D COF thin films with an anisotropic "face-on" arrangement. Both *ex situ* concentration- and time-dependent studies have uncovered an unusual re-entrant transition in the orientation during the COF thin film growth. The appearance of a disoriented phase is correlated with a kinetically-delayed, solution-based COF growth process. The first appearance of the oriented phase at the earlier stage of growth and the disappearance of the disoriented phase at a later stage suggest a strong interface-initiated templating effect that benefits from the reversibility of the crosslinking chemistry. This is the first experimental observation that a disoriented phase, in addition to disordered phases, occurs as an intermediate state during the thin film growth of COFs. More importantly, the reversibility of the imine bond allows kinetically grown and misorientedly attached COF layers to undergo error-checking and self-correction to reinstate vertical orientation to the substrate. It is plausible to use concentrations and reaction time as effective handles to address certain crystalline phases in a COF thin film. It should be noted that the domain sizes of crystallites grown under the conditions studied are limited to ~20–30 nm as a result of the competition between in-plane and out-of-plane growth processes. Further optimization of COF thin film growth conditions is desired to minimize the inferior domain boundaries.[24] Nevertheless, the successful fabrication of highly oriented thin films from a combination of interfaces and dynamic covalent chemistry validates an important step towards the integration of 2D COF thin films as electroactive materials for next generation optoelectronic devices. The optimization and integration of such oriented films for field effect charge transport measurement are currently ongoing.

Acknowledgements

This work was performed at the Molecular Foundry, and X-ray studies were carried out at BL 7.3.3 and 11.0.1.2 at Advanced Light Source (ALS). Both the Molecular Foundry and ALS are user facilities supported through the Office of Science, Office of Basic Energy Sciences, the U.S. Department of Energy, under Contract No. DE-AC02-05CH11231. B. H. and Y. L. are supported by the Inorganic–Organic Nanocomposites program under the same contract number. H. W. is grateful to the Chinese Scholarship Council and National Postdoctoral

Program for Innovation Talents for fellowships. H. W. and T. T. acknowledge the support from the National Basic Research Program of China (973 program: 2013CB733600) and the National Nature Science Foundation of China (Grant No. 21436002, 21390202). F. L. and T. P. R. were supported by the Laboratory Directed Research and Development Program of Lawrence Berkeley National Laboratory under U.S. Department of Energy Contract No. DE-AC02-05CH11231. S. C. is grateful to the support from the National Nature Science Foundation of China (Grant No. 21603076).

Notes and references

1 (*a*) J. W. Colson and W. R. Dichtel, *Nat. Chem.*, 2013, **5**, 453–465; (*b*) A. P. Côté, A. I. Benin, N. W. Ockwig, M. O'Keeffe, A. J. Matzger and O. M. Yaghi, *Science*, 2005, **310**, 1166–1170; (*c*) X. Feng, X. Ding and D. Jiang, *Chem. Soc. Rev.*, 2012, **41**, 6010–6022; (*d*) S.-Y. Ding and W. Wang, *Chem. Soc. Rev.*, 2013, **42**, 548–568.

2 (*a*) P. J. Waller, F. Gándara and O. M. Yaghi, *Acc. Chem. Res.*, 2015, **48**, 3053–3063; (*b*) L. Ascherl, T. Sick, J. T. Margraf, S. H. Lapidus, M. Calik, C. Hettstedt, K. Karaghiosoff, M. Doeblinger, T. Clark, K. W. Chapman, F. Auras and T. Bein, *Nat. Chem.*, 2016, **8**, 310–316.

3 D. D. Medina, V. Werner, F. Auras, R. Tautz, M. Dogru, J. Schuster, S. Linke, M. Döblinger, J. Feldmann, P. Knochel and T. Bein, *ACS Nano*, 2014, **8**, 4042–4052.

4 (*a*) S. Jin, X. Ding, X. Feng, M. Supur, K. Furukawa, S. Takahashi, M. Addicoat, M. E. El-Khouly, T. Nakamura, S. Irle, S. Fukuzumi, A. Nagai and D. Jiang, *Angew. Chem., Int. Ed.*, 2013, **52**, 2017–2021; (*b*) M. Calik, F. Auras, L. M. Salonen, K. Bader, I. Grill, M. Handloser, D. D. Medina, M. Dogru, F. Loebermann, D. Trauner, A. Hartschuh and T. Bein, *J. Am. Chem. Soc.*, 2014, **136**, 17802–17807; (*c*) S. Jin, T. Sakurai, T. Kowalczyk, S. Dalapati, F. Xu, H. Wei, X. Chen, J. Gao, S. Seki, S. Irle and D. Jiang, *Chem. – Eur. J.*, 2014, **20**, 14608–14613; (*d*) S.-L. Cai, Y.-B. Zhang, A. B. Pun, B. He, J. Yang, F. M. Toma, I. D. Sharp, O. M. Yaghi, J. Fan, S.-R. Zheng, W.-G. Zhang and Y. Liu, *Chem. Sci.*, 2014, **5**, 4693–4700; (*e*) G. H. V. Bertrand, V. K. Michaelis, T.-C. Ong, R. G. Griffin and M. Dincă, *Proc. Natl. Acad. Sci. U. S. A.*, 2013, **110**, 4923–4928; (*f*) S. Lin, C. S. Diercks, Y.-B. Zhang, N. Kornienko, E. M. Nichols, Y. Zhao, A. R. Paris, D. Kim, P. Yang, O. M. Yaghi and C. J. Chang, *Science*, 2015, **349**, 1208–1213.

5 (*a*) D. N. Bunck and W. R. Dichtel, *J. Am. Chem. Soc.*, 2013, **135**, 14952–14955; (*b*) S. Mitra, S. Kandambeth, B. P. Biswal, A. Khayum M, C. K. Choudhury, M. Mehta, G. Kaur, S. Banerjee, A. Prabhune, S. Verma, S. Roy, U. K. Kharul and R. Banerjee, *J. Am. Chem. Soc.*, 2016, **138**, 2823–2828; (*c*) S. Chandra, S. Kandambeth, B. P. Biswal, B. Lukose, S. M. Kunjir, M. Chaudhary, R. Babarao, T. Heine and R. Banerjee, *J. Am. Chem. Soc.*, 2013, **135**, 17853–17861.

6 (*a*) N. A. A. Zwaneveld, R. Pawlak, M. Abel, D. Catalin, D. Gigmes, D. Bertin and L. Porte, *J. Am. Chem. Soc.*, 2008, **130**, 6678–6679; (*b*) S. Clair, M. Abel and L. Porte, *Chem. Commun.*, 2014, **50**, 9627–9635.

7 L. Xu, X. Zhou, Y. Yu, W. Q. Tian, J. Ma and S. Lei, *ACS Nano*, 2013, **7**, 8066–8073.

8 (*a*) T. Brezesinski, J. Wang, S. H. Tolbert and B. Dunn, *Nat. Mater.*, 2010, **9**, 146–151; (*b*) J. Yang, D. Yan and T. S. Jones, *Chem. Rev.*, 2015, **115**, 5570–5603.

9 (*a*) J. W. Colson, A. R. Woll, A. Mukherjee, M. P. Levendorf, E. L. Spitler, V. B. Shields, M. G. Spencer, J. Park and W. R. Dichtel, *Science*, 2011, **332**, 228–231; (*b*) E. L. Spitler, J. W. Colson, F. J. Uribe-Romo, A. R. Woll, M. R. Giovino, A. Saldivar and W. R. Dichtel, *Angew. Chem., Int. Ed.*, 2012, **51**, 2623–2627.

10 D. D. Medina, J. M. Rotter, Y. Hu, M. Dogru, V. Werner, F. Auras, J. T. Markiewicz, P. Knochel and T. Bein, *J. Am. Chem. Soc.*, 2015, **137**, 1016–1019.

11 R. P. Bisbey, C. R. DeBlase, B. J. Smith and W. R. Dichtel, *J. Am. Chem. Soc.*, 2016, **138**, 11433–11436.

12 Y. Chen, H. Cui, J. Zhang, K. Zhao, D. Ding, J. Guo, L. Li, Z. Tian and Z. Tang, *RSC Adv.*, 2015, **5**, 92573–92576.

13 C. R. DeBlase, K. Hernández-Burgos, K. E. Silberstein, G. G. Rodríguez-Calero, R. P. Bisbey, H. D. Abruña and W. R. Dichtel, *ACS Nano*, 2015, **9**, 3178–3183.

14 S.-Y. Ding, J. Gao, Q. Wang, Y. Zhang, W.-G. Song, C.-Y. Su and W. Wang, *J. Am. Chem. Soc.*, 2011, **133**, 19816–19822.

15 F. L. Geyer, A. Pun, D. Hanifi, U. H. F. Bunz and Y. Liu, *J. Mater. Chem. C*, 2013, **1**, 6661–6666.

16 A. Hexemer, W. Bras, J. Glossinger, E. Schaible, E. Gann, R. Kirian, A. MacDowell, M. Church, B. Rude and H. Padmore, *J. Phys.: Conf. Ser.*, 2010, **247**, 012007.

17 B. E. Warren, *X-ray Diffraction*, Dover Publications, Inc., New York, 1990.

18 T. Threlfall, *Org. Process Res. Dev.*, 2003, **7**, 1017–1027.

19 S. Kandambeth, V. Venkatesh, D. B. Shinde, S. Kumari, A. Halder, S. Verma and R. Banerjee, *Nat. Commun.*, 2015, **6**, 6786.

20 (*a*) Q. Hu, M. H. Nielsen, C. L. Freeman, L. M. Hamm, J. Tao, J. R. I. Lee, T. Y. J. Han, U. Becker, J. H. Harding, P. M. Dove and J. J. De Yoreo, *Faraday Discuss.*, 2012, **159**, 509–523; (*b*) J. J. De Yoreo and P. G. Vekilov, *Rev. Mineral. Geochem.*, 2003, **54**, 57–93.

21 B. J. Smith, A. C. Overholts, N. Hwang and W. R. Dichtel, *Chem. Commun.*, 2016, **52**, 3690–3693.

22 Q. Gao, L. Bai, Y. Zeng, P. Wang, X. Zhang, R. Zou and Y. Zhao, *Chem. – Eur. J.*, 2015, **21**, 16818–16822.

23 B. J. Smith and W. R. Dichtel, *J. Am. Chem. Soc.*, 2014, **136**, 8783–8789.

24 J. I. Feldblyum, C. H. McCreery, S. C. Andrews, T. Kurosawa, E. J. G. Santos, V. Duong, L. Fang, A. L. Ayzner and Z. Bao, *Chem. Commun.*, 2015, **51**, 13894–13897.